ISSN 1069-3513, Izvestiya, Physics of the Solid Earth, 2022, Vol. 58, No. 4, pp. 445–458. © The Author(s), 2022. This article is an open access publication.
Russian Text © The Author(s), 2022, published in Fizika Zemli, 2022, No. 4, pp. 3–18.

Recent Volumetric Deformations of Fault Zones

Yu. O. Kuzmin*

Schmidt Institute of Physics of the Earth, Russian Academy of Sciences, Moscow, 123242 Russia
**e-mail: kuzmin@ifz.ru*

Received February 18, 2022; revised February 21, 2022; accepted February 22, 2022

Abstract—Volumetric (non-shear) deformations of fault zones measured from leveling data are analyzed. It is shown that volumetric deformations within fault zones lead to symmetric local surface subsidence. Examples of anomalous subsidence identified in the Ashgabat fault zone (North Kopet Dag) and in the fault zones of the underground gas storage facility are presented. A mechanism describing the formation of these anomalous deformations based on the models of poroelastic inclusion and poroelastic inhomogeneity is proposed. The problem about surface displacements of elastic halfspace with a poroelastic region in the form of vertical extended rectangular prism simulating active fragment of a fault zone is solved. Analytical formulas for surface-displacement estimation are derived for two variants of poroelastic models: a model of inclusion and a model of heterogeneity. The comparison of the two models based on the case study of the Ashgabat fault has shown that the mechanism of anomalous deformations with poroelastic heterogeneity model much better describes the observed displacements than poroelastic inclusion model. The analysis of anomalous surface displacements at an underground gas storage facility indicates that local subsidence occurs during both gas withdrawal and injection. It is established that the formation of anomalous subsidence in the first case follows the poroelastic inclusion model, and in the second case it corresponds to the poroelastic heterogeneity model. This means that local subsidence in a fault zone during gas withdrawal is linearly related to the change in reservoir pressure. Anomalous subsidence during gas injection is nonlinearly linked to the change in reservoir pressure. This is a striking example of induced deformations in the fault zones when temporal variations of poroelastic parameters within a fault zone in the setting of external quasistatic loading induce local perturbation in the stress-strain state of rocks in the vicinity of fault.

Keywords: volumetric deformations, fault zone, poroelastic inclusion, poroelastic heterogeneity, underground gas storage facility

DOI: 10.1134/S1069351322040061

INTRODUCTION

It is traditionally believed that recent deformations of fault zones are formed by shear displacements. Depending on the type of relative block displacement and the dip angle of the fault plane, faults are classified into normal, reverse, thrust, strike-slip, and transient (oblique) forms (normal faults with a shear component, shears with normal fault component, etc.). According to Anderson's theory of faulting, there are three main types of faults: normal, strike-slip, and reverse faults (Turcotte and Schubert, 2002). In accordance with the principles of mechanics of deformable media, all the above fault types refer to pure shear displacements of fault sides.

However, fracture mechanics considers three main mechanisms of fracture (fracture modes): opening mode, in-plane shear, and out-of-plane shear. Thus, there are only two genetic types of fracture: opening and shear. Therefore, in a number of works on structural geology and geomechanics, kinematics of fault motion is described not only by shears but also by tensile faults (joints) (Gzovskii, 1975; Sherman, 1977; Davis, 1983; Okada, 1985; 1992; Yang and Davis, 1986; Peacock, 2016).

Recent shear deformations of fault zones are ubiquitously detected as coseismic and postseismic displacements in the focal zones of strong earthquakes (Kocharyan, 2016; Scholz, 2019). Recent deformations in the zones of tensile faults in the form of local subsidence of the Earth's surface have detected based on the results of high-precision leveling observations in seismic and oil and gas regions (Kuzmin, 1999; 2014; 2021a; 2021b). An important fact is that most of the revealed anomalies are associated with fluid-saturated faults and the kinematics of vertical displacements is a symmetric subsidence in the vicinity of the fault zones. These anomalies are observed almost ubiquitously. The main prerequisite for their detection is the presence of an observation network with benchmark spacing of at most 1 km. In the vast majority of cases, these anomalies are local subsidence (Kuzmin, 2018a; 2018b).

From the principles of mechanics of deformable medium it follows that total deformation consists of

two constituents: volumetric and shear. In this case, any "non-shear" deformations of the medium can be considered volumetric. From that perspective, the observed symmetric, local surface subsidence or elevations are manifestations of volumetric deformations of fault zones.

The presence of fluid-saturated faults substantially determines the volumetric type of deformation of fault zones. Naturally, this requires consideration of the mechanisms of anomalous surface deformation based on poroelastic model of the medium. This paper presents the analysis of several anomalous deformations of the Earth's surface based on the notions of poroelastic inclusions and poroelastic heterogeneities as model analogs of volumetric deformation of fault zones.

MECHANISM OF VOLUMETRIC DEFORMATION OF FAULT ZONES BASED ON POROELASTIC INCLUSION AND POROELASTIC HETEROGENEITY MODELS

As a formation mechanism of local surface subsidence arising in the zones of tensile faults, three geomechanical models—block, dislocation, and parametrically induced—are typically considered (Kuzmin, 2019).

As comparative analysis shows, the block model where a horizontal pulling-apart between basement blocks is specified and surface subsidence of a sedimentary layer takes place fails to meet two empirical facts. This model does not predict local anomalies. The width of anomalies depends on the ratio between the sizes of basement blocks and thickness of sedimentary layer. But what is most important is the condition that time variations of horizontal block displacements correspond to time behavior of local near-fault subsidence and that amplitudes of the latter are commensurate with block displacement amplitudes. Meanwhile, this is not observed in the measurement results. Besides, block models do not form local volumetric strains within fault zones.

The dislocation model fairly well describes local features of near-fault surface displacements. For example, tensile jumps of displacements in the fault predicted by the model are quite comparable with the observed values. However, dislocation models are substantially flawed in that their faults have no width. Moreover, in a dislocation model, the morphology and amplitude of anomalous surface displacements in fault zone does not depend on the pattern and intensity of regional ("external") conditions in which a local anomaly develops. A characteristic feature of the distribution of vertical displacements is that subsidence amplitude is commensurate with the amplitude of surface uplift. Such phenomena have never been observed in the real data.

Although block and dislocation models provide symmetric surface subsidence, these models cannot be fully identified with volumetric deformations developing within the fault zone. Moreover, it is difficult to describe fluid-saturated faults in these models. For example, in (Verma et al., 2017), a tensile dislocation is placed in a poroelastic half-space and, therefore, cannot be identified with a fluid-saturated fault.

A parametrically induced model postulates that local deformation processes recorded by repeated detailed geodetic observations in fault zones are caused by "internal" factors (time variations in stiffness parameters of a fault zone), while regional processes provide a quasi static background of applied stresses the pattern of which determines specific morphology of the resulting anomalies. An important point is that to simulate the observed magnitudes of anomalous strains (5×10^{-5}–10^{-4} yr^{-1}), it is sufficient to drive the model by the conditions of as small as few percent time variation in the fault stiffness parameters (elastic moduli) within local segments of the initially stressed fault zones. It is in this model that elastic medium can be naturally generalized into poroelastic medium.

Most geomechanical models describing local strain anomalies consider elastic half-space containing a three-dimensional (3D) finite-volume region which undergoes volumetric strain ε_0. The surface of the half-space, identified with the ground surface, is considered to be stress free. Different authors identify this volumetric deformation as *transformational strain* or *inclusion* (Eshelby, 1961), *eigenstrain* (Mura, 1987), *nuclei of strain* (Mindlin and Cheng, 1950), and *distortion* (Nowacki, 1986). All the definitions have in common that ε_{ij}^0 is an anomalous deformation with respect to the hosting medium, which does not meet the condition of compatibility of strains. I refer to this deformation as distortion, the term widely used in the works of V. Nowacki devoted to inhomogeneous problems of thermal elasticity.

As it is known (Eshelby, 1961), anomalous deformations can be estimated either by solving the problem about inclusion or the problem about heterogeneity (inhomogeneity). The main difference between these problems is that in the first case, external loads on the half-space are typically absent. In the problems of surface displacements of a half-space containing an heterogeneity of mechanical properties, anomalous deformations are formed in the conditions of external loading. In some particular cases, these problems admit equivalent solutions, e.g., in the case of a variation in the bulk moduli within the inclusion (Tsurkis and Kuzmin, 2022). If we consider a poroelastic inclusion as a model describing the formation of volumetric deformations in fault zones, we can initially use the model of elastic inclusion and then generalize the obtained solutions to poroelastic inclusion. In a similar way, the solution of the problem with elastic heterogeneity can be generalized into the solution of the problem with poroelastic heterogeneity.

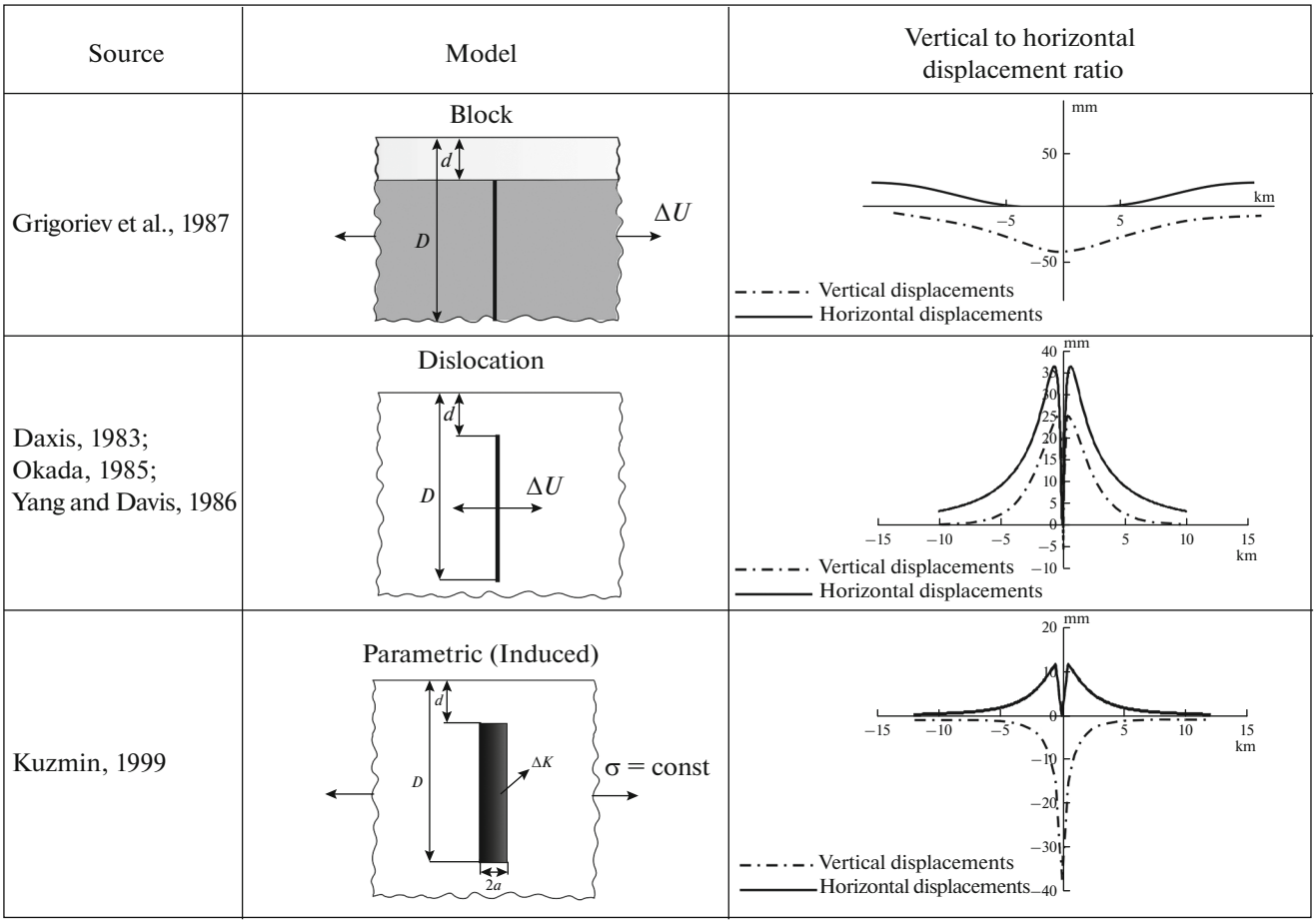

Fig. 1. Comparison of vertical and horizontal surface displacements for different fault models.

Figure 2 schematically illustrates the difference between boundary conditions in the cases when deformation of a fault zone is described by the models of inclusion and heterogeneity.

The figure shows how local volumetric deformations are formed in the cases of elastic and poroelastic inclusions and heterogeneity In fault zones without fluid, anomalous surface displacements are formed by local volumetric strains ε^0. When faults are fluid saturated, volumetric deformations are created by the changes in pore (formation) pressure ΔP. Similarly, in the problem of elastic heterogeneity, anomalous volumetric deformations arise at a change in the bulk modulus ΔK. In the presence of a fluid-saturated fault, anomalous volumetric strains within an activated segment of a fault zone occur at a change in the pore volume compressibility ΔC_p. It is this way that the transition from elastic models of an inclusion and heterogeneity to poroelastic models is carried out.

In the linear theory of elasticity, stress σ_{ij} is linked with strain ε_{ij} by Hooke's law $\sigma_{ij} = C_{ijkl}\varepsilon_{ij}$ where C_{ijkl} is the tensor of elastic moduli. For isotropic medium, Hooke's law can be expressed in the following form:

$$\sigma_{ij} = 2\mu\varepsilon_{ij} + \left(K - \frac{2\mu}{3}\right)\delta_{ij}e. \quad (1)$$

Here, $e = \varepsilon_{kk}$ is volumetric strain; μ is shear modulus; K is bulk modulus; δ_{ij} is Kronecker delta ($\delta_{ij} = 1$, at $i = j$, and $\delta_{ij} = 0$, at $i \neq j$). Strain ε_{ij} satisfies the Cauchy formula:

$$\varepsilon_{ij} = \left(\frac{1}{2}\right)\left(u_{i,j} + u_{j,i}\right). \quad (2)$$

For quasi static processes when forces of inertia can be neglected, stress σ_{ij} should satisfy the equilibrium conditions in the following form:

$$\sigma_{ij,i} + F_j(x,t) = 0, \quad (3)$$

where $F_j(x,t)$ is a volume or mass force (body force). Substituting (1) and (2) into (3) we obtain the equilibrium equation expressed in terms of displacement gradients:

$$\left(K + 2\mu/3\right)e_{,j} + \mu u_{j,kk} + F_j(x,t) = 0. \quad (4)$$

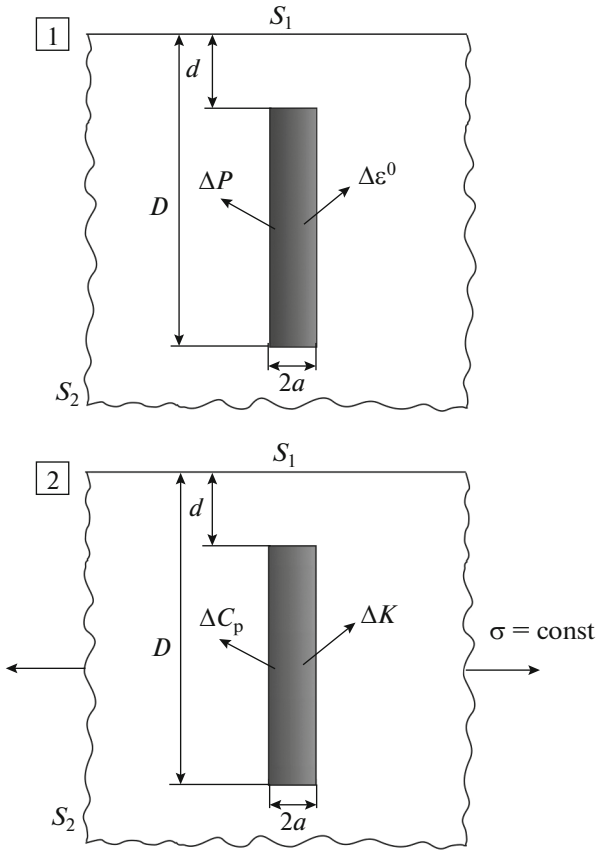

Fig. 2. Geometric scheme of local volumetric deformations of fault zones in problem with inclusion (1) and heterogeneity (2).

Formula (1) of Hooke's law is written using elastic moduli K and μ. To simplify transformations, this formula can be recast in terms of elastic moduli λ and μ, where λ is the Lamé parameter, in the following form:

$$\sigma_{ij} = 2\mu\varepsilon_{ij} + \lambda\delta_{ij}e. \tag{5}$$

In contrast to formula (1), the shear modulus in Eq. (5) is present in the term containing shear strain, and the Lamé parameter is present in the term containing volumetric strain. Moduli λ and K are connected by the relation $\lambda = \dfrac{3K - 2\mu}{3}$.

To solve the problem, the Betti's reciprocal work theorem (Sokolnikoff, 1956) generalized for elastic bodies with distortions (Novacki, 1986) was used. If there are two systems of causes (surface T_i and mass forces F_i, stresses σ_{ij}) and effects (displacements u_i and distortions ε_{ij}^0), then the work done by the forces of the first system through displacements and distortions produced by the second system of forces is equal to the work done by the second system of forces through the displacements and distortions produced by the first system of forces:

$$\int_V (F_i u_i' - F_i' u_i)dV + \int_S (T_i u_i' - T_i' u_i)dS + \int_V (\sigma_{ij}'\varepsilon_{ij}^0 - \sigma_{ij}\varepsilon_{ij}'^0)dV = 0. \tag{6}$$

Here, the prime symbols mark the surface and mass forces and the stresses and distortions of the second system. The reciprocal work theorem (6) allows us to derive methods for integration of equations in displacements. Using the theorem, we can find surface displacement caused by the first system of the applied forces from the known solution which is used at the action of the second system of forces. In this case, Maysel's method (Maysel, 1941) is employed, in which for finding vertical surface displacements of a semi-infinite elastic body, the known solution for the displacements produced by the application of a vertical point load to the surface is used as the second system of forces.

As the first system, a semi-infinite body where only distortions ε_{ij}^0 are acting is considered. Let the mass forces be zero. We assume that the surface of the body consists of two parts: part S_1 coinciding with the stress-free surface of the Earth and part S_2 which occupies the rest of the area and is fixed. Thus, there are no stresses on S_1 and no displacements on S_2. As the second (primed) system, we consider the same body, stress free on S_1 and fixed on S_2. We assume then that there are no distortions ($\varepsilon_{ij}'^0 = 0$) in the body and that the concentrated force $F_i' = \delta(x - \xi)\delta_{ik}$ acts at point ξ in the direction of the x_k-axis. This force causes displacements $u_i' = G_i^{(k)}(x, \xi)$ which should satisfy the equilibrium equations:

$$\mu\Gamma_{i,jj}^{(k)} + (\lambda + \mu)G_{j,ji}^{(k)} + \delta(x - \xi)\delta_{ik} = 0, \tag{7}$$

with boundary conditions

$$G_i^{(k)} = 0, \quad x \in S_2,$$
$$T_i^{(k)} = \left[\mu(G_{j,i}^{(k)} + G_{i,j}^{(k)}) + \delta_{ij}G_{j,j}^{(k)}\right]n_j = 0, \quad x \in S_1. \tag{8}$$

In formulas (7) and (8), $\delta(x - \xi)$ and $G_i^{(k)}$ are Dirac and Green's functions, respectively. Knowing the Green's function for half-space, we can calculate arising stresses σ_{ij}':

$$\sigma_{ij}' = \mu(G_{i,j}^{(k)} + G_{j,i}^{(k)}) + \lambda\delta_{ij}G_{j,j}^{(k)}. \tag{9}$$

The solution of Eq. (7) with boundary conditions (8) is a typical problem of static elasticity theory for a body without distortion. Applying the reciprocal work theorem (6) to both systems of causes and effects, we obtain the following equation:

$$-\int_V \delta(x-\xi)\delta_{ik}u_i(x)\,dV(x) + \int_V \sigma'^{(k)}_{ij}(x,\xi)\varepsilon^0_{ij}(x)\,dV(x) = 0. \quad (10)$$

The substitution of boundary conditions into (10) gives a formula that links surface displacement and distortion through the known value of the Green's function for stresses $\sigma'^{(k)}_{ij}(x,\xi)$:

$$u_k(\xi) = \int_V \varepsilon^0_{ij}(x)\sigma'^{(k)}_{ij}(x,\xi)\,dV(x), \quad k = 1,2,3. \quad (11)$$

Thus, we found the displacements $u_k(\xi)$ expressed integrally through distortions. Under the integral sign is the known distortion distribution and stresses $\sigma'^{0}_{ij}(x,\xi)$ caused by the action of the concentrated force, directed along the x_k-axis, at point ξ. Given that for our problem the distortion should be specified in the form of volumetric strain ε^0, then $\varepsilon^0_{ij} = \delta_{ij}\varepsilon^0$. Thus, taking into account Eq. (9), we obtain the equation for $u_k(\xi)$:

$$u_k(\xi) = 3K\int_V \varepsilon^0(x)G^{(k)}_{j,j}(x,\xi)\,dV(x). \quad (12)$$

Here, $G^{(k)}_{j,j}(x,\xi)$ is the Green's function for displacements.

If we consider only vertical displacements $u_3(\xi)$, then Eq. (12) has the following form

$$u_3(\xi) = 3K\int_V \varepsilon^0(x)G^{(3)}_{j,j}(x,\xi)\,dV(x). \quad (13)$$

In the most compact form, the Green's tensor from a vertical concentrated force applied to the surface of a half-space is described by the following formulas (Converse and Comninou, 1975):

$$G^3_1 = \frac{\xi_1 - x_1}{4\pi\mu}\left(\frac{\xi_3}{R^3} - \frac{1-2\nu}{R(R+\xi_3)}\right),$$
$$G^3_2 = \frac{\xi_2 - x_2}{4\pi\mu}\left(\frac{\xi_3}{R^3} - \frac{1-2\nu}{R(R+\xi_3)}\right), \quad (14)$$
$$G^3_3 = \frac{1}{4\pi\mu}\left(\frac{2(1-\nu)}{R} + \frac{\xi_3^2}{R^3}\right),$$

where $\xi_1\xi_2\xi_3$ are coordinates of the point in the inclusion (distortion region). If, for convenience, we change variables ($\xi_1 - x_1 = x$, $\xi_2 - x_2 = y$, $\xi_3 = z$) and differentiate the obtained expression with respect to the corresponding coordinates, we obtain:

$$G^3_{1,1} + G^3_{2,2} + G^3_{3,3} = -\frac{(1-2\nu)Z}{2\pi\mu R^3}. \quad (15)$$

Substituting (14) into (15), we obtain the formula for estimating vertical surface displacements of elastic half-space:

$$U_3 = \frac{3(1-2\nu)K\varepsilon^0}{2\pi\mu}\int_V \frac{ZdXdYdZ}{R^3}. \quad (16)$$

In (16) there is no minus sign before the fraction because the z-axis is directed towards the interior of the half-space. This formula can also be used for estimating horizontal displacements if we replace the variable z in the numerator of the integrand by x or y, respectively. To obtain analytical formulas, Eq. (16) should be integrated over the volume of the activated fragment of the fault zone.

If we now introduce in our analysis a medium with a poroelastic inclusion which simulates a fluid-saturated fault, then, following Goodier (1937), Geertsma (1957), Zimmerman (1991) and Wang (2000) who have consistently demonstrated the analogy between elastic and thermoelastic phenomena and between thermoelastic and poroelastic strains, we may show that $\varepsilon^0 = \frac{\alpha P}{3K} = 1/3\, mC_p\, P$ where α is the Biot number; m is formation porosity; K is the bulk modulus; and ΔP is the change in (formation) pore pressure. Substituting these values into formula (17) and considering that $K = \frac{2\mu(1+\nu)}{3(1-2\nu)}$, we obtain the final formula for estimation of vertical surface displacements at a change in reservoir pressure in a fault zone:

$$U_3 = \frac{(1+\nu)mC_p\,\Delta P}{3\pi}\int_V \frac{ZdXdYdZ}{R^3}. \quad (17)$$

To describe the geometry of the fault zone, it is proposed to use a model of vertical elongated prism (Fig. 3), as is common in geological and geophysical fault models.

From (17) we can see that the formula for vertical displacements can be represented in the form of a product of two factors $U_3 = PhGe_3$, where Ph is a physical factor characterizing displacement intensity, and Ge_3 is a geometric factor describing the morphology of the spatial distribution of vertical displacements depending on the shape of inclusion (distortion).

In (Kuzmin, 1999) it was established that, to solve Eq. (17), one can use a gravideformational analogy which is based on the fact that geometric factor completely coincides with the integral formula for vertical gradient of gravitational potential $W, z = g$:

$$\Delta g = -f\Delta\rho\int_V \frac{ZdXdYdZ}{R^3}, \quad (18)$$

where f is gravitational constant and $\Delta\rho$ density change. The comparison of Eqs. (17) and (18) proves the gravideformational analogy. Then we can use the well-known solution of the potential theory for the anomaly Δg of a prismatic body which has an anomalous density relative to the density of ambient rocks and is located at depth from the surface of the half-

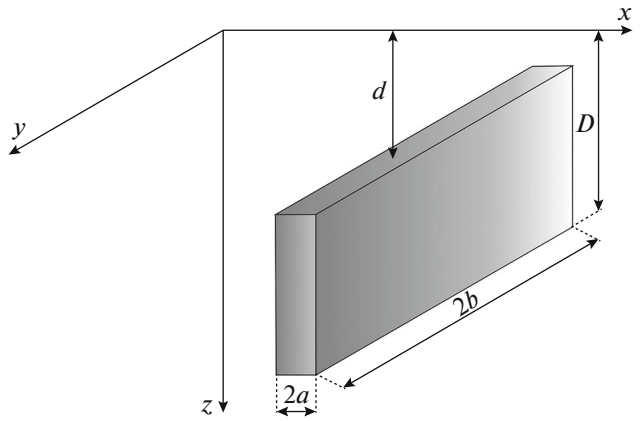

Fig. 3. Shape and geometric parameters of fault model.

space. This solution can be found in the reference books and textbooks on gravity prospecting, e.g., in (Mironov, 1972).

For example, in the case of a plane problem, when $2b \to \infty$, the formula for vertical displacements U_3 is following:

$$U_3 = \left[\frac{(1+\nu)\, m C_p\, \Delta P}{3\pi}\right] \times \left[(x+a)\ln\frac{(x+a)^2+d^2}{(x+a)^2+D^2} - (x-a) \times \ln\frac{(x-a)^2+d^2}{(x-a)^2+D^2} - 2D\left(\arctan\frac{x+a}{D} - \arctan\frac{x-a}{D}\right) + 2d\left(\arctan\frac{x+a}{d} - \arctan\frac{x-a}{d}\right)\right]. \quad (19)$$

Due to awkwardness, the full analytical formula for the volumetric problem is not presented here, but it also consists of a combination of functions ln and arctan.

Remarkably, the use of Eq. (17) is not limited to describing fault zone deformations but the formula can also be used to model surface displacements associated with oil-and-gas reservoir development. When the prism width (2a) is (much) greater than thickness $(D - d)$, it is a model of a producing formation. When the prism width is (much) smaller than thickness, it is a model of a fault zone. Because volumetric strain is a small value, we can use the principle of linear superposition and obtain a displacement field in the case when oilfield consists of several layers. In a similar way, it is possible to construct a field of vertical displacements from a system of faults located within one oilfield.

In (Kuzmin, 1999), I considered a heterogeneity model which was used to estimate vertical surface displacements of an elastic half-space with a fault zone where bulk moduli differ from those of the host medium. The model also uses the reciprocal work theorem and the assumption of small (percent and first tens of percent) relative changes in the bulk modulus. The range of relative variations in elastic moduli was assumed to be small in the same measure as the assumption of small deformations underlying the linear elasticity theory.

As shown by numerous observations, local subsidence in the zones of tensile faults occurs in the setting of horizontal extension (Kuzmin, 2014; 2018a; 2018b; 2018c). In this case, the formula for estimating vertical displacements in a zone of a tensile fault is following:

$$U_3 = \frac{\mathcal{H}(1-2\nu)\,\sigma_{11}}{6\pi\mu}\int_V \frac{ZdXdYdZ}{R^3}. \quad (20)$$

Here $\mathcal{H} = \frac{\Delta K}{K}$. With decreasing $\mathcal{H}$, for example, the land surface will subside, because also in this case, the Z-axis is directed downwards and, therefore, if $\mathcal{H} < 0$, $\sigma_{11} < 0$ (tensile stresses), then $U_3 > 0$.

To generalize the above formula to the case of poroelastic inhomogeneity, it is necessary to introduce poroelastic coefficients in it. This can be done in the following way. As the temporal variation in bulk modulus K occurs within the poroelastic medium of the fault zone, this modulus characterizes the integral characteristic of the poroelastic volume. Then, following (Soltanzadeh et al., 2007; Segall, 2010), we may consider macroscopic variation of the bulk modulus without considering its microscopic characteristics. In this case, K characterizes the ratio between the applied effective confining pressure ΔP_{eff} and the relative volumetric deformation of the pore space $\frac{\Delta V_p}{V_p}$, where V_p is the volume of the pore space of the fault zone.The integral bulk modulus of the poroelastic medium can be then denoted by K_p.

The theory of poroelastic media widely uses a reciprocal of K_p. This quantity is referred to as a compressibility coefficient of the pore space C_p and is defined by formula (21):

$$C_p = \frac{1}{\Delta P_{eff}}\frac{\Delta V_p}{V_p}. \quad (21)$$

The effective pressure for rocks with porosity higher than 5% is determined by the difference between confining compression and pore pressure: $P_{eff} = P_c - P_p$ where P_c is confining pressure. For the conditions of the upper crust, confining pressure is equal to lithostatic pressure, and the pore pressure is equivalent to the formation pressure.

The analysis of formula (21) shows that pore compressibility decreases with a decline in the formation pressure and increases with its rise. Given that $K_p = \frac{1}{C_p}$, the bulk modulus will increase with the reduction in the formation pressure and decrease with the increase in P_p. In this case, local subsidence in the zone of a fluid saturated fault which is in the state of quasi static horizontal extension will be observed at the increase in formation pressure. This situation is fundamentally different from the fault model in the form of a poroelastic inclusion, in which the increase in formation pressure leads to the uplift of the land surface.

VOLUMETRIC DEFORMATIONS IN THE ZONE OF ASHGABAT FAULT

Almost all authors note that the recent geodynamics of the Turkmenian–Iranian segment of the Alpine folded belt is formed by the convergence (collision) of the Turan and Iranian plates. In the north, the region of interaction of these plates is limited by the Peredovoi (forefront) Kopet Dag (Ashgabat) fault which simultaneously constitutes the northern boundary of Kopet Dag. The latter overthrusts the Predgornyi depression (Pre-Kopet Dag foredeep), and the Ashgabat fault obliquely plunges beneath Kopet Dag. The dip (the angle of inclination in the vertical plane) of this fault is, on average, approximately 50° to 70° (the angle with the downward vertical line is from 20° to 40°) in different cross sections. The amplitude of vertical displacements along the fault reaches 5–7 km. Besides, right-lateral horizontal displacements are observed on the Ashgabat fault, reaching 30 km over the period of their Neotectonic evolution (Kalugin, 1977; Trifonov, 1978; Allen et al., 2008).

In this case, at the present stage, the tectonic structures composing the Turkmenian–Iranian segment of the Earth's crust should have the following kinematics of horizontal displacements in the meridional direction. The NNE motion of the Arabian Plate leads to the formation of the collision zone between the Iranian and Turan microplates, Kopet Dag thrusting over the Turan platform, and right-lateral shear displacement along the Ashgabat fault.

If we follow this scheme and assume that recent crustal movements are fully inherited from the past geological epochs, then that the existing system of deformational observations in the central part of the northern Kopet Dag which has been making measurements for more than 50 years should have confidently detected systematic NNE surface tilting of the foothill land regions from leveling data and a consistent increase in the length of the baselines intersecting the Kopet Dag Ashgabat fault at an angle of 45° and less (Kuzmin, 2021a).

However, annual average horizontal strains in the Ashgabat fault zone estimated from geodetic data proved to be 2×10^{-8} yr^{-1}. Moreover, if we compare horizontal displacement velocities derived from optical distance measurements and geological data, then, based on the long-term geodetic observations (over about 50 years), the velocity of right-lateral shear displacement on the Ashgabat fault is 1/133 of the corresponding value estimated from geological data!

The similar data were also obtained by the study of vertical surface displacements based on repeated high-precision leveling. Observations were conducted on a system of five profiles intersecting the Ashgabat fault zone. The observations covered a fault segment 80 km long. Over the observation period (58 years), the average rate of vertical displacements on the Kopet Dag Ashgabat fault (Kopet Dag thrusting) is 0.07 mm/yr. If we consider the notion of a surface tilt as a horizontal gradient of vertical displacements, we obtain the average rate of surface tilting in the Ashgabat fault zone at 2.5×10^{-8} yr^{-1}. Such a low strain rate (10^{-8} yr^{-1}) indicates that the average annual rate of change of regional stresses is extremely low. If we assume that the strain rate is linearly proportional to the rate of applied stresses, then, with a typical stiffness of the medium, the rate of temporal changes in regional stresses will be on the order of 100 Pa/yr. This is a surprising result if we consider the fact that the strain estimates are derived from geodetic observations in the seismically active region.

It is interesting to compare the obtained strain rates surface tilts with the Earth's tide which is a reference geodynamic process. For examples, for the geographic coordinates of Ashgabat, the amplitude of deformations induced by lunar semidiurnal wave *M2* which is dominant throughout the spectrum of tidal waves is $\sim 2.3 \times 10^{-8}$ for tidal tilts and 1.6×10^{-8} for horizontal tidal strains, respectively. In this case, the average relative strain rate in a seismically active region is at most 1–2 amplitudes of Earth tidal deformations per year. This means that the Iranian–Turan segment of the collision zone of the Arabian and Eurasian plates has been in the state of quasi static (soft) loading for the last 50 years. At the same time, local aseismic deformation anomalies with the rates of 10^{-5} yr^{-1} have been repeatedly recorded in the fault zones in Northern Iran (Saberi et al., 2017) and in Southern Turkmenistan (Kuzmin, 2014; 2018a; 2018b; 2019).

For a more detailed analysis of the correlation between regional and local processes in the Ashgabat fault zone, we can consider the results of the long-term precise leveling observations (Fig. 4) along the profile intersecting the fault in the region of Ashgabat. The profile is divided into two sections: a 4-km long "block" section located beyond the fault zone and a "fault" section with a length of 0.6 km selected directly in the fault zone. The levelings were repeated monthly. The height difference measurement results are converted into tilts by the division by the distance between benchmarks.

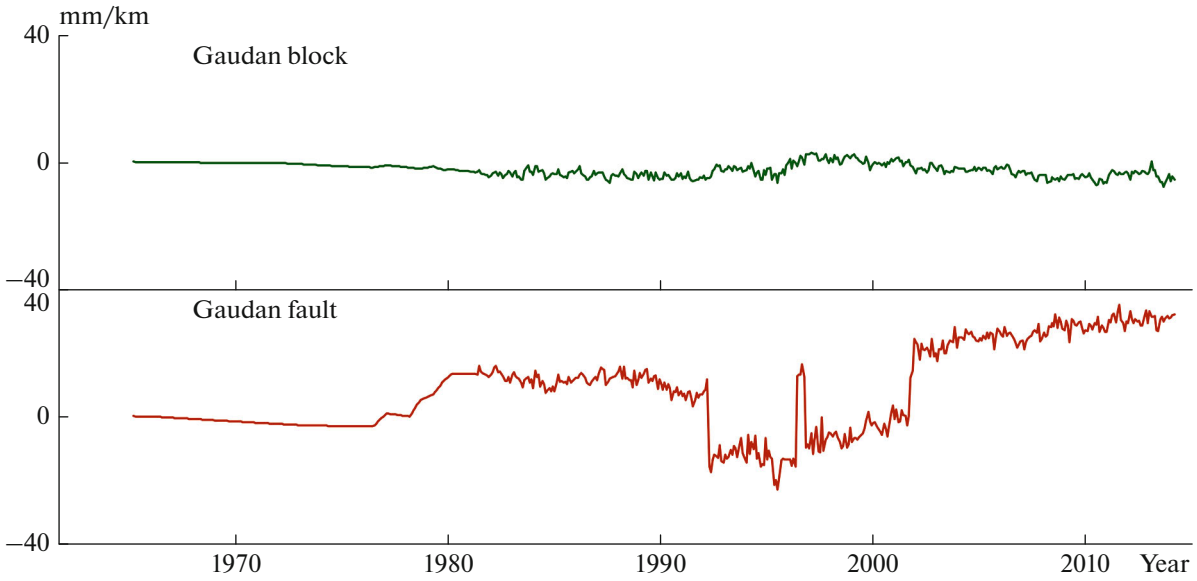

Fig. 4. Time behavior of vertical surface displacements at geodynamic test site Gaudan in block part of profile and within Ashgabat fault.

From the graph it can be seen that against the weak background trend there are alternating-sign variations of movements, reaching the rates on the order of 5×10^{-7} yr^{-1} for the flank part and 10^{-5} yr^{-1} for the fault zone. From this it follows that local deformations in the fault zone occur under the conditions of quasi static (background) loading. The fault zone manifests itself autonomously as the durations of anomalous deformation periods in the block and fault do not coincide.

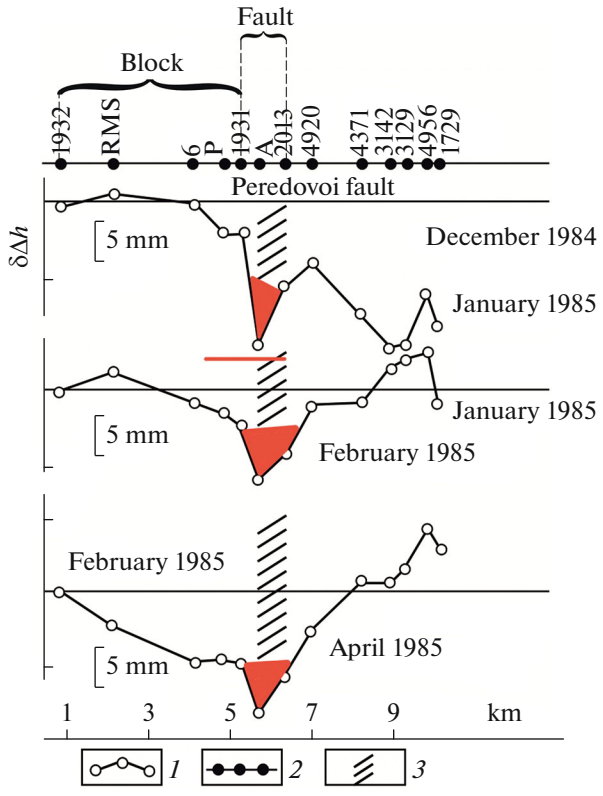

Fig. 5. Spatial distribution of recent vertical surface displacements in Ashgabat fault zone. (*1*) Vertical displacements along profile; (*2*) observation points; (*3*) fault zone.

The spatial distribution of vertical surface displacements can be analyzed based on Fig. 5 which depicts the results of leveling observations on the same profile intersecting the Ashgabat fault. The distance between benchmarks reaches here a few hundred meters, and the time period between successive leveling is one month.

The figure shows that the γ-type anomalous surface displacements (subsidence) with amplitude of ~5 mm and width 0.5–1.0 km are observed in the fault zone. This is a typical morphology of the recent geodynamics of faults, identified by numerous geodetic measurements in many regions of the world (Kuzmin, 1999; 2019). If we sum up the cumulative vertical displacements and estimate the rate of relative deformations (tilting), it will be 6×10^{-5} yr^{-1}.

Figure 6 shows the results of periodogram analysis (Kuzmin and Fattakhov, 2021), the leveling results obtained along the entire Gaudan profile, along the block section, and within the local fault section of this profile. The periods were calculated using a special program WinABD for time series processing developed at IPE RAS (Desherevskii et al., 2016a; 2016b).

In order to eliminate the "scaling" effect, vertical benchmark displacements were converted into relative deformations by dividing by the length of the corresponding profiles.

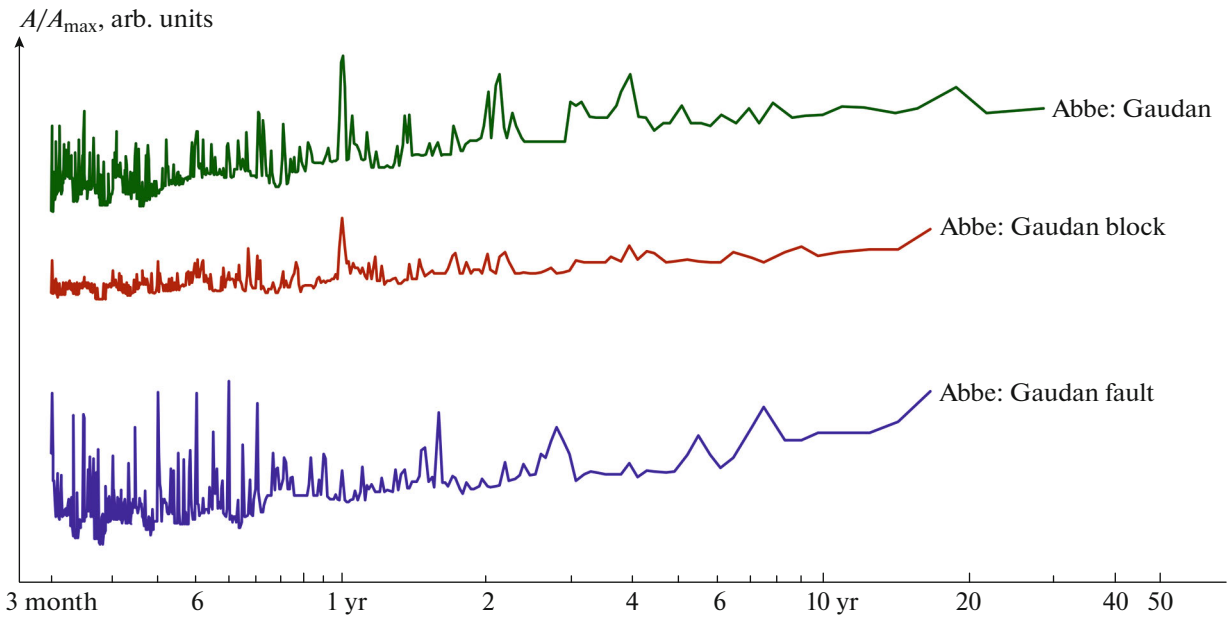

Fig. 6. Abbe periodogram of leveling results along Gaudan profile for different sections.

As follows from the figure, the leveling results for the block section and for the entire Gaudan profile (14 km) indicate the presence of a dominant seasonal (annual) constituent in the spectrum of vertical displacements. The periodogram obtained from the leveling data on the fault section is drastically different. There is almost no dominance of the annual harmonic in this periodogram; the most pronounced harmonics appear in the region of shorter periods. This fact is additional evidence in favor of autonomous manifestation of anomalous deformations in the fault zone.

Figure 7 shows the leveling results for the block and fault sections and the results of continuous tilt measurements in a specially arranged room at a depth of 25 m with tiltmeters having a sensitivity of an order of angular millisecond (5×10^{-9}).

In fact, the comparison was carried out for three tiltmeters - two in the flank zones (Figs. 7a and 7b) and one directly in the vicinity of the fault zone (Fig. 7c). These data were compared with precipitation variations recorded by the Gauda weather station directly in Kopet Dag about 30 km south of the observation system (Kuzmin, 1999).

From Fig. 7 it follows that the leveling results and tilt data obtained in the flank parts on different sides of the fault zone agree well. Their trend variations are insignificant and vary within 0.2–0.3 angular seconds (about 10^{-7} yr^{-1}) over the incomplete nine years. Against the almost imperceptible trend, the annual (thermoelastic) surface tilts are clearly observed. Hence, the regional stress field did not experience significant temporal changes over the considered time interval (about 10 years), i.e., temporal activation of the regional endogenous impact was minimal.

At the same time, as suggested by Fig. 7c, the character of surface deformation in the near-fault zone is fundamentally different. The behavior of the curve is clearly irregular. The amplitudes of anomalous variations reach 1.5–2.0 angular seconds (about 10^{-5}) and in their temporal structure there are oscillations with periods from 3–4 to 2–2.5 years. Evidently, the fault zone has its own, local dynamics with its own temporal structure and anomalously high deformation level.

What is most important is that the temporal structure of the deformation process in the fault zone strongly correlates with the precipitation behavior (Fig. 7d) recorded by the Gaudan weather station located in the mountains approximately ~40 km to the south of the fault zone. The analysis of the hydrogeological conditions has shown that the near-fault, deep groundwater is fed by atmospheric precipitation falling within a drainage area in the mountains where the weather station is located. In this case, periodic rises and falls in the level of precipitation that falls in the mountains and drains off into the fault zone modulate pore pressure of the near-fault fluid, which may lead to deformations of the fault zone (Kuzmin, 2019).

It should be noted that during the entire period of instrumental observations within the measurement network of the Ashgabat geodynamic test site, there were no strong earthquakes. Individual seismic events with $M \leq 6$ occurred but did not cause trend changes in the time series of observations. Anomalous deformations induced by the preparation processes of these earthquakes were typically local in time. After the seismic events occurred, the temporal behavior of defor-

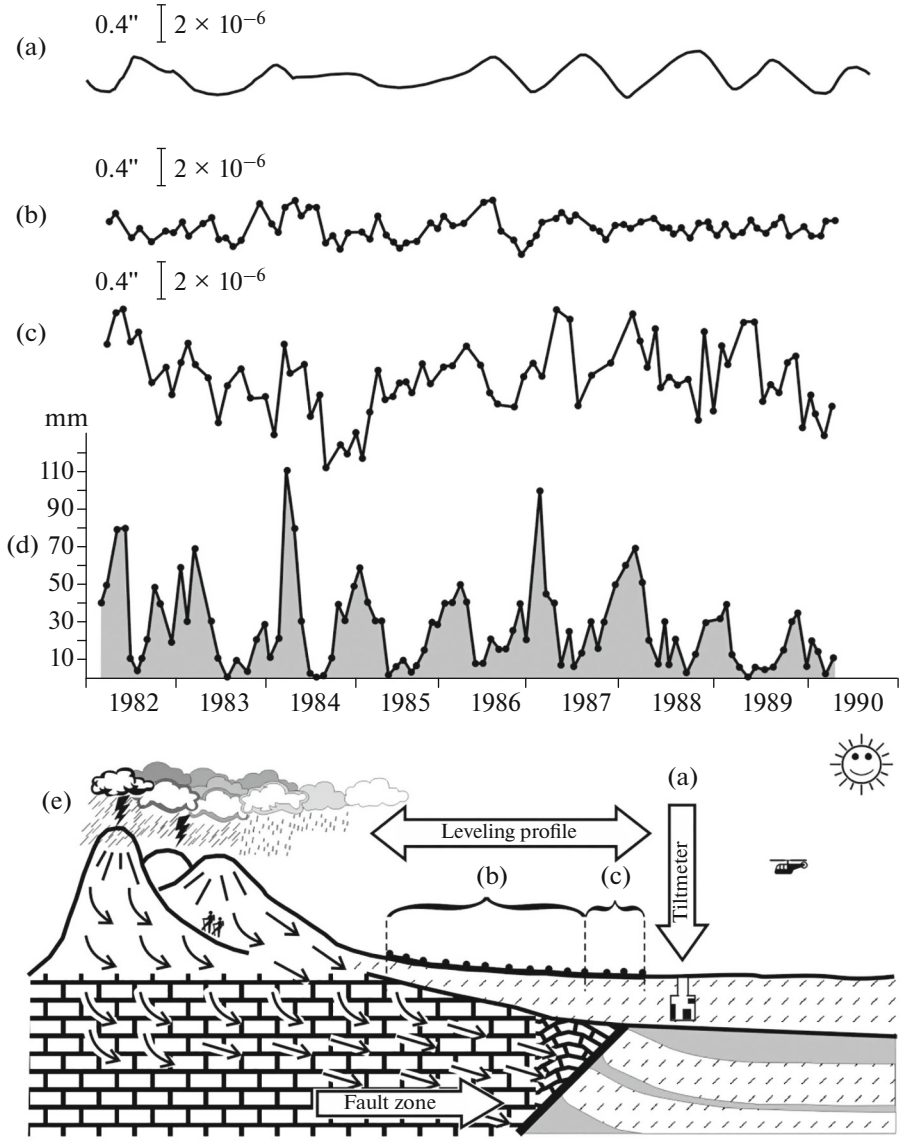

Fig. 7. Time behavior of surface tilt and precipitation: (a) tiltmeter observations; (b) leveling data within block; (c) leveling results within fault zone; (d) precipitation at weather station "Gaudan;" (e) layout of measurement systems on profile.

mations recovered at the background level (Kuzmin, 1999; 2021a).

Formula (17) describes anomalous displacement arising at a change in volumetric deformation of the fluid-saturated medium of the fault due to a change in the pore fluid pressure caused by precipitation fluctuation, and formula (20) describes anomalous displacements arising at a change in the bulk modulus due to precipitation dynamics, when the external regional stress is quasi static. Thus, on a qualitative level, both mechanisms can explain the high correlation between variations in the precipitation level and anomalies in the temporal behavior of vertical displacements measured from the leveling data on the fault section of the profile.

To determine which mechanism is dominant, we need to compare formulas (17) and (20). If we accept the natural assumption that fault zone in both mechanisms has the same geometric parameters, then the geometric factors in both formulas are identical. Therefore, we can compare the contribution of each mechanism to the formation of local displacements on the fault using the ratio of the physical coefficients.

The regional stress state of the upper part of the Earth's crust is (horizontally) extensional because the Kopet Dag thrust on the Turan microplate forms the Pre-Kopet Dag foredeep whose southern slope is in the state of subhorizontal extension (Sidorov and Kuzmin, 1989).

The analysis of long-term tidal observations in the Ashgabat fault zone has shown the presence of anomalous variations in tidal tilts. The estimates by the method of S.M. Molodenskii (1983) indicate that relative changes in the bulk modulus of the fault zone $\mathcal{H}$, which form anomalous variations in the amplitudes of tidal tilts can range between 1 and 3% (Kuzmin, 1999).

Assuming for comparative estimation the typical parameter values $\nu = 0.25$, $m = 0.1$, $C_p = 10^{-3}$ MPa^{-1}, $\Delta P = 100$ mm of water (10^3 Pa), $\mu = 10^4$ MPa, $\sigma_{11} = 100$ MPa, $\mathcal{H} = 0.01$, we can calculate the values of the physical factors for the problem with inclusion (Ph_{inc}) and heterogeneity (Ph_{het}). Substituting the above parameter values we obtain the Ph_{het} value a factor of $\sim 10^3$ larger than Ph_{inc}.

Thus, the dominant mechanism forming the anomalous displacements in the fault zone under the influence of atmospheric precipitation is the fluctuations in the bulk modulus of the fluid saturated medium associated with the variations in the pore fluid pressure in the fault, i.e., the mechanism of poroelastic heterogeneity.

VOLUMETRIC DEFORMATIONS OF FAULT ZONES DURING OPERATION OF A UNDERGROUND GAS STORAGE FACILITY

An underground gas storage (UGS) is a test object with well known geological model and amplitude of cyclic loading. By conducting repeated geodetic observations one can determine surface deformation response to the changes in reservoir pressure. In autumn and winter, gas is withdrawn from the storage, and in spring and summer, injected into it. The mandatory strict control of facility's tightness and volumes of injected and withdrawn gas ensures high degree of exploration of main UGS parameters: geometric dimensions and configuration of the object, physical properties of rocks, and amplitude of cyclic variation in reservoir pressure. The specificity of UGS operation is that a geological object is an aquifer or a depleted gas field.

We discuss the underground storage organized in the depleted reservoir in the gas field. The reservoir is located at a depth of about 2 km. During the operation, the gas storage is twice a year subjected to cyclic loading due to gas injection and withdrawal. The change in pressure at depth during the geodetic measurements is from 0.8 MPa (withdrawal) to 1.1 MPa (injection).

Figure 8 shows the results of repeated leveling along one profiles at the Stepnovskoe underground gas storage facility in the European part of Russia (Kuzmin, 2021b). Leveling observations are repeated, on average, bi-annually. In the interval between the observations conducted during the gas withdrawal period, the general behavior of the curve shows the subsidence in the central part of the gas storage facility. During the gas injection period, the ground surface uplifts in the central part of the profile.

The estimate of relative deformations along the entire profile ("background" strain component) indicates that the alternating-sign vertical surface displacements are 1.3×10^{-6} during both withdrawal and injection periods. The strain amplitude in the fault zones varies from 2×10^{-5} to 8.7×10^{-5}. Thus, fault zones intensify cyclic deformations during operation of the underground gas storage by almost a factor of 15.

If we number the faults from left to right, then we see that the local anomalies associated with fault no. 1 are characterized by local subsidence during the periods of gas withdrawal and vanish during injection. Fault no. 2 does not manifest itself during withdrawal but is marked by local subsidence during injection. Local displacements in the vicinity of fault no. 3 behave in the similar way. During withdrawal, the subsidence is observed, whereas during injection, the benchmark fixed to the fault again sinks. This means that the deformation response of faults to cyclic loads is nonlinear not only in strain amplitude but also in the sign of anomalous displacements. On all three faults, local subsidence is observed during the period when either gas withdrawal or injection takes place.

The results of the leveling observations show that during gas withdrawal, a general subsidence of the entire territory of the underground gas storage facility and local subsidence in the fault zones takes place. These processes are adequately described by the poroelastic inclusion model (17). At gas injection, a general surface uplift and local subsidence in the fault zones occur. General uplift corresponds to the inclusion model which however does not permit local subsidence in the fault zones. But if we use the poroelastic heterogeneity model for the fault zones (20), then it is possible to adequately describe the obtained results in the case of gas injection.

The underground gas storage facility is a depleted gas field. The field is hosted by an anticlinal uplift. In this case, the upper half of the upward-bending layer is in a setting of subhorizontal extension and the lower half in compression. As noted above, with the rise in pore pressure in the fluid saturated medium of the fault zone, the pore compressibility coefficient C_p increases leading to a decrease in relative effective stiffness ($\mathcal{H}$) which forms local subsidence under the action of horizontal extension ($\sigma_{11} < 0$) caused by activation of bending. This means that the sources of anomalies are confined to the activated fragments of the fault zones located above the neutral bending axis. Thus, the deformation processes develop, which correspond to different models of anomalous deformations. For example, the local subsidence in the first fault zone during gas withdrawal corresponds to the poroelastic inclusion model, and the subsidence on

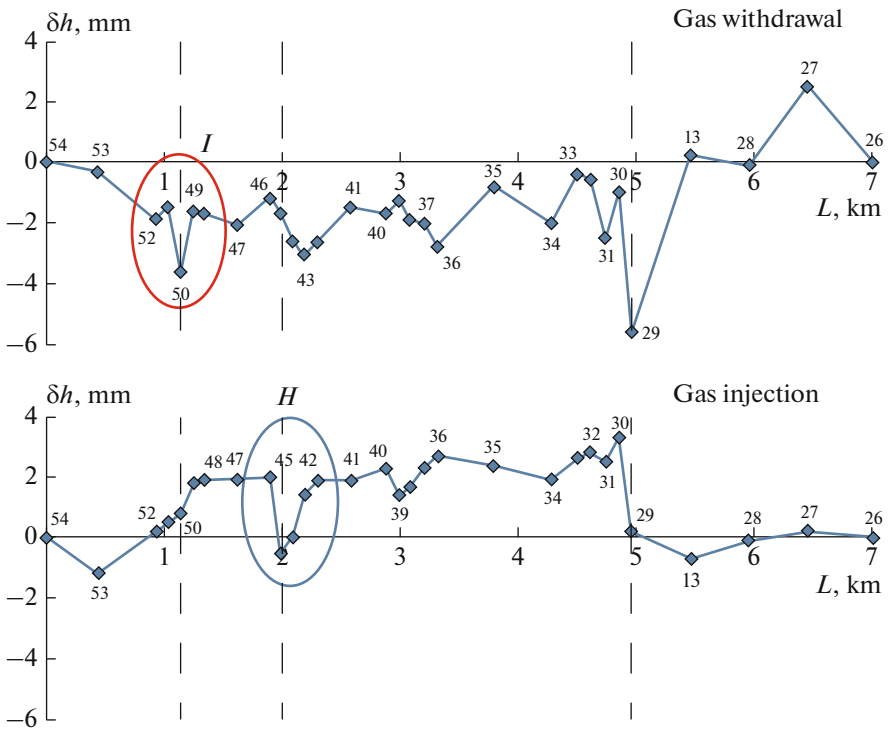

Fig. 8. Vertical surface displacements at underground gas storage facility. Dashed lines show of fault locations identified from geological and geophysical data. Ovals mark anomalies corresponding to inclusion model (*I*) and inhomogeneity model (*H*).

the second fault during gas injection can be described by the poroelastic inhomogeneity model, which is indicated in the figure.

As follows from the figure, subsidence amplitudes in both cases are approximately equal. Subsidence widths are also commensurate up to the distance between benchmarks. Then, if we assume that the geometrical parameters of the anomaly sources are approximately equal, the proposed mechanisms will be valid provided approximately equal physical factors in formulas (17) and (20), which are dimensionless quantities.

Assuming for phenomenological estimating $\Delta P = 0.8$ MPa, $\nu = 0.25$, $m = 0.1$, $C_p = 10^{-3}$ MPa^{-1}, $\mu = 10^4$ MPa, we obtain the physical factor $Ph_{\text{inc}} = 0.9 \times 10^{-5}$.

To estimate the physical factor Ph_{het} we have to estimate and σ_{11} in formula (20). In (Zhukov and Kuzmin, 2021) in the experiments on samples of reservoir rock from a number of gas fields and underground gas storages it was shown that at a change in pore pressure by 1 MPa, the pore compressibility coefficient C_p increased and the bulk modulus K_P decreased. The relative change in the bulk modulus $\mathcal{H}$ was about 1%.

To estimate the magnitude of horizontal extension σ_{11}, we can use thin plate theory as a bent-layer' length is much larger than its thickness. Convenient formulas are presented in a well-known book (Turcotte and Shubert, 2002). From this theory it follows that the stresses can be approximately estimated by the following formula:

$$\sigma_{11} \cong \frac{2.3KHh}{L^2}, \qquad (22)$$

where H is the thickness of the bending layer; L is the horizontal dimension of the underground gas storage; h is amplitude of anticlinal uplift. Using (22) and the data on the geological structure of the Stepnovskoe gas storage, we can estimate the horizontal extension formed by anticlinal uplift over the geological time. It proved to be $\sigma_{11} \cong 40$ MPa. Substituting these values into formula (20), we estimate $Ph_{\text{het}} = 1.2 \times 10^{-5}$.

Thus, combining the models of poroelastic inclusion and poroelastic inhomogeneity, we can analyze the entire spectrum of the observed vertical movements of the Earth's surface.

CONCLUSIONS

The study has shown that local surface deformations are not formed throughout the entire fault zone but localized within spatially limited activated fault segments. Local symmetric subsidence and uplifts of the Earth's surface are clearly not shear if shear displacement is understood in the mechanical rather than geological meaning.

The developed concepts of poroelastic inclusions and inhomogeneities as sources of local surface displacements advanced to the level of quantitative models made it possible to select the mechanisms of anomalous deformations in the Ashgabat fault zone and to determine the problem about a rectangular poroelastic inhomogeneity simulating an activated fragment of a fault zone to be the dominant model.

The analysis of the spatial distribution of surface deformations at the underground gas storage facility has shown that local subsidence in the fault zones occurs both at withdrawal and injection. It is established that in the first case, the formation of anomalous subsidence according follows the model of poroelastic inclusion, and in the second case, the model of poroelastic inhomogeneity. This means that local subsidence in the fault zone during gas extraction is linearly related to the changes in reservoir pressure.

The formation of anomalous subsidence during gas injection is nonlinearly related to the changes in reservoir pressure. This is a striking example of induced deformations of fault zones when temporal variations of poroelastic parameters within a fault zone in the setting of external quasi static loads form a local perturbation of the stress-strain state in the vicinity of the fault.

The proposed quantitative models are largely phenomenological. Unfortunately, the detailed data on the interior structure of the fault zones are clearly insufficient to develop more complex models that capture microscopic characteristics of faults. In my opinion, in this situation, the degree of model detail should be kept strictly corresponding to the level of detail and quality of the empirical material. As the empirical data become more extensive and detailed, the models will become more complex.

FUNDING

The work was carried out in partial fulfillment of state contract of the Schmidt Institute of Physics of the Earth of the Russian Academy of Sciences.

CONFLICT OF INTEREST

The author declares that he has no conflicts of interest.

OPEN ACCESS

REFERENCES

Allen, M., Jacson, J., and Walker, R., Late Cenozoic reorganization of the Arabia-Eurasia collision and the comparison of short-term and long-term deformations rates, *Tectonics*, 2004, vol. 23, no. 2, Paper ID TC2008.

Converse, G. and Comninou, M., Dependence on the elastic constants of surface deformation due to faulting, *Bull. Seismol. Soc. Am.*, 1975, vol. 65, no. 5, pp. 1173–1176.

Davis, P.M., Surface deformation associated with a dipping hydrofracture, *J. Geophys. Res.*, 1983, vol. 88, pp. 5826–5834.

Deshcherevsky, A.V., Zhuravlev, V.I., Nikolsky, A.N., and Sidorin, A.Ya., Technologies for analyzing geophysical time Series: Part 1. Software requirements, *Seism. Instrum.*, 2017a, vol. 53, no. 1, pp. 46–59.

Deshcherevsky, A.V., Zhuravlev, V.I., Nikolsky, A.N., and Sidorin, A.Ya., Technology for analyzing geophysical time series: Part 2. WinABD—A software package for maintaining and analyzing geophysical monitoring data, *Seism. Instrum.*, 2017b, vol. 53, no. 3, pp. 203–223.

Eshelby, J.D., Elastic inclusions and inhomogeneities, in *Progress in Solid Mechanics*, vol. 2, Sneddon, I.N. and Hill, R., Eds., Amsterdam: North-Holland, 1961, pp. 87–140.

Geertsma, J., A remark on the analogy between thermoelasticity and the elasticity of saturated porous media, *J. Mech. Phys. Solids*, 1957, vol. 6, no. 1, pp. 13–16.

Goodier, J.N., On the integration of the thermoelastic equations, *Philos. Mag., Ser. 7*, 1937, vol. 23, no. 157, pp. 1017–1032.

Gzovsky, M.V., *Osnovy tektonofiziki* (Basics of Tectonophysics), Moscow: Nauka, 1975.

Kalugin, P.I., *Yuzhnyi Kopetdag (geologicheskoe opisanie)* (Southern Kopetdag: Geological Characgterization)), Ashkhabad: Ylym, 1977.

Kocharyan, G.G., *Geomekhanika razlomov* (Geomechanics of Faults), Moscow: GEOS, 2016.

Kuzmin, Yu.O., *Sovremennaya geodinamika i otsenka geodinamicheskogo riska pri nedropol'zovanii* (Recent Geodynamics and Geodynamic Risk Assessment in Subsoil Use), Moscow: Agentstvo Ekonom. Nov., 1999.

Kuzmin, Yu.O., Recent geodynamics of fault zones: faulting on real-time scale, *Geodinam. Tektonofiz.*, 2014, vol. 5, no. 2, pp. 401–443.

Kuzmin, Yu.O., Recent anomalous surface deformation in fault zones: shear or tensile faulting?, *Geodinam. Tektonofiz.*, 2018a, vol. 9, no. 3, pp. 967–987.

Kuzmin, Yu.O., Recent geodynamics of tensile faults, *Izv., Phys. Solid Earth*, 2018b, vol. 54, no. 6, pp. 886–903.

Kuzmin, Yu.O., Induced deformations of fault zones, *Izv., Phys. Solid Earth*, 2019, vol. 55, no. 5, pp. 753–765.

Kuzmin, Yu.O., Deformation consequences of the development of oil and gas field, *Izv., Atmos. Ocean. Phys.*, 2021a, vol. 57, no. 11, pp. 1479–1497.

Kuzmin, Yu.O., Geodynamical evolution of the Earth's crust of Central Asia and recent geodynamics of the Kopet Dag region, Turkmenistan, *Izv., Phys. Solid Earth*, 2021b, vol. 57, no. 1, pp. 131–139.

Kuzmin, Yu.O. and Fattakhov, E.A., Analysis of the time structure of strain processes in the Ashgabat fault zone (Northern Kopet Dag), *Seism. Prib.*, 2022, vol. 58, no. 2, pp. 148–159.

Mandl, G., *Rock Joints. The Mechanical Genesis*, Berlin: Springer, 2005.

Maysel, V.M., A generalization of the Betti-Maxwell theorem to the case of thermal stresses and some of its applications, *Dokl. Akad. Nauk. SSSR*, 1941, vol. 30, pp. 115–118.

Mindlin, R.D. and Cheng, D.H., Nuclei of strain in the semi-infinite solid, *J. Appl. Phys.*, 1950, vol. 21, no. 9, pp. 926–933.

Mironov, V.S., *Kurs gravirazvedki* (Course in Gravity Prospecting), Leningrad: Nedra, 1980.

Molodenskii, S.M., On local anomalies in amplitudes and phases of tidal tilts and strains, *Izv. Akad. Nauk SSSR, Fiz. Zemli*, 1983, no. 7, pp. 3–9.

Mura, T., *Micromechanics of Defects in Solids*, 2nd ed., Norwell: Kluwer, 1987.

Nowacki, W., *Thermoelasticity*, 2nd ed., Warsaw: PWN, 1986.

Okada, Y., Surface deformation due to shear and tensile faults in a half-space, *Bull. Seismol. Soc. Am.*, 1986, vol. 75, no. 4, pp. 1135–1154.

Okada, Y., Internal deformation due to shear and tensile faults in a half-space, *Bull. Seismol. Soc. Am.*, 1992, vol. 82, no. 2, pp. 1018–1040.

Peacock, D.C.P., Nixon, C.W., Rotevatn, A., Sanderson, D.J., and Zuluaga, L.F., Glossary of fault and other fracture networks, *J. Struct. Geol.*, 2016, vol. 92, pp. 12–29.

Saberi, E, Yassaghi, A., and Djamour, Y., Application of geodetic leveling data on recent fault activity in Central Alborz, Iran, *Geophys. J. Int.*, 2017, vol. 211, pp. 773–787.

Scholz, C.H., *The Mechanics of Earthquakes and Faulting*, Cambridge: Cambridge Univ. Press, 2019.

Segall, P., *Earthquake and Volcano Deformation*, Princeton: Princeton Univ. Press, 2010.

Sherman, S.I., *Fizicheskie zakonomernosti razvitiya razlomov zemnoi kory* (Physical Regularities in the Development of Crustal Faults), Novosibirsk: Nauka.1977.

Sidorov, V.A. and Kuzmin, Yu.O., *Sovremennye dvizheniya zemnoi kory osadochnykh basseinov* (Recent Movements of the Earth's Crust of Sedimentary Basins), Moscow: Nauka, 1989.

Sokolnikoff, S., *Mathematical Theory of Elasticity*, 2nd ed., New York: McGraw-Hill, 1956.

Soltanzadeh, H., Hawkes, C.D., and Sharma, J.S., Poroelastic model for production and injection-induced stresses in reservoirs with elastic properties different from the surrounding rock, *Int. J. Geomech.*, 2007, vol. 7, no. 5, pp. 353–361.

Trifonov, V.G., Late Quaternary tectonic movements of western and central Asia, *Geol. Soc. Am. Bull.*, 1978, vol. 89, pp. 1059–1072.

Tsurkis, I.Ya. and Kuzmin, Yu.O., Stress state of an elastic plane with one or more inclusions of arbitrary shape: the case of identical shear moduli, *Mech. Solids*, 2022, vol. 57, no. 1, pp. 34–48.

Turcotte, D.L. and Shubert, G., *Geodynamics*, 2nd ed., Cambridge: Cambridge Univ. Press, 2002.

Verma, H., Swaroop, R., and Kumar, V., Deformation of poroelastic half-space due to tensile dislocation, *Int. J. Eng. Sci. Res. Technol.*, 2017, vol. 6, no. 12, pp. 115–124.

Wang, H.F., *Theory of Linear Poroelasticity with Applications to Geomechanics and Hydrology*, Princeton: Princeton Univ. Press, 2000.

Yang, X.M. and Davis, P.M., Deformation due to a rectangular tensile crack in an elastic half-space, *Bull. Seismol. Soc. Am.*, 1986, vol. 76, pp. 865–881.

Zhukov, V.S. and Kuzmin, Yu.O., Experimental estimation of compressibility coefficients for fractures and intergranular pores of an oil and gas reservoir, *Zap. Gorn. Inst.*, 2021, vol. 251, pp. 658–666.

Zimmerman, R., *Compressibility of Sandstones*, Amsterdam: Elsevier, 1991.

Translated by M. Nazarenko